

## RESEARCH ARTICLE

# Exogenous expression of caveolin-1 is sufficient for hepatic stellate cell activation

Mariana Ilha<sup>1</sup>  | Ketlen da Silveira Moraes<sup>1</sup> | Francieli Rohden<sup>1</sup>  |  
 Leo Anderson Meira Martins<sup>1</sup>  | Radovan Borojevic<sup>2</sup>  | Guido Lenz<sup>3</sup>  |  
 Florencia Barbé-Tuana<sup>1,4</sup>  | Fátima Costa Rodrigues Guma<sup>1,5</sup> 

<sup>1</sup>Programa de Pós-Graduação em Ciências Biológicas- Bioquímica, Instituto de Ciências Básicas da Saúde, Universidade Federal do Rio Grande do Sul – UFRGS, Porto Alegre, RS, Brazil

<sup>2</sup>Centro de Medicina Regenerativa, Faculdade de Medicina de Petrópolis – FMP, Petrópolis, RJ, Brazil

<sup>3</sup>Departamento de Biofísica e Centro de Biotecnologia, Universidade Federal do Rio Grande do Sul - UFRGS, Porto Alegre, RS, Brazil

<sup>4</sup>Programa de Pós-Graduação em Biologia Celular e Molecular, Escola de Ciências da Pontifícia Universidade Católica do Rio Grande do Sul- PUCRS, Porto Alegre, RS, Brazil

<sup>5</sup>Centro de Microscopia e Microanálise, Universidade Federal do Rio Grande do Sul - UFRGS, Porto Alegre, RS, Brazil

## Correspondence

Mariana Ilha, Departamento de Bioquímica, Instituto de Ciências Básicas da Saúde, UFRGS, Rua Ramiro Barcelos, 2600 – anexo, CEP 90035-003 Porto Alegre, RS, Brazil.  
 Email: mariana.ilha@ufrgs.br

## Funding information

Ministério da Ciência e Tecnologia, Grant/Award Number: 423712/2016-0; Coordenação de Aperfeiçoamento de Pessoal de Nível Superior; Fundação de Amparo à Pesquisa do Estado do Rio Grande do Sul, Grant/Award Number: 1952-2551/13; Pró-Reitoria de Pesquisa, Universidade Federal do Rio Grande do Sul; Conselho Nacional de Desenvolvimento Científico e Tecnológico, Grant/Award Number: 423712/2016-0; CNPq; CAPES; MCT/ CNPq Universal, Grant/Award Number: 423712/2016-0; PqG/FAPERGS, Grant/Award Number: 1952-2551/13; PROPESQ-UFRGS

## Abstract

Caveolin-1 (Cav-1) expression is increased in hepatic stellate cells (HSC) upon liver cirrhosis and it functions as an integral membrane protein of lipid rafts and caveolae that regulates and integrates multiple signals as a platform. This study aimed to evaluate the role of Cav-1 in HSC. Thus, the effects of exogenous expression of Cav-1 in GRX cells, a model of activated HSC, were determined. Here, we demonstrated through evaluating well-known HSC activation markers – such as  $\alpha$ -smooth muscle actin, collagen I, and glial fibrillary acidic protein – that up regulation of Cav-1 induced GRX to a more activated phenotype. GRX<sup>EGFP-Cav1</sup> presented an increased migration, an altered adhesion pattern, a reorganization f-actin cytoskeleton, an arrested cell cycle, a modified cellular ultrastructure, and a raised endocytic flux. Based on this, GRX<sup>EGFP-Cav1</sup> represents a new cellular model that can be an important tool for understanding of events related to HSC activation. Furthermore, our results reinforce the role of Cav-1 as a molecular marker of HSC activation.

## KEYWORDS

caveolae, caveolin-1, GRX, hepatic stellate cells activation, liver fibrosis, molecular marker

## 1 | INTRODUCTION

Chronic liver diseases (CLDs) have a large impact on public health expenditures, significantly contributing to human mortality rates.<sup>1</sup> Worldwide, 844 million people have CLDs with a lethality rate of 2 million deaths per year.<sup>2</sup> Liver fibrosis is a characteristic of several CLDs, such as nonalcoholic fatty liver disease,

viral hepatitis, nonalcoholic steatohepatitis, cirrhosis, and liver cancer and it is defined by the excessive release of extracellular matrix (ECM).<sup>1</sup> Moreover, liver has a unique competence to adapt to damage through tissue repair. The imbalance of ECM release by hepatic scarring leads to significant changes in architectural and organ function, making it dangerous and clinically significant.<sup>3</sup>

Hepatic stellate cells (HSC) are the major orchestrators of liver fibrosis by producing and altering the ECM in acute injury of liver. Through stimuli of hepatic damage, these cells are activated to a more proliferative and fibrogenic phenotype, transforming their quiescent phenotype to a cell with classic myofibroblast characteristics.<sup>4</sup> Indeed, HSC control the turnover of liver connective tissue regulating homeostasis of ECM and also participating in contractility of hepatic sinusoids.<sup>5</sup> Besides the morphological changes,<sup>6</sup> some hallmarks of HSC activation include the reduction on levels of intracellular lipid droplets, increase on the production of ECM, alpha-smooth muscle actin ( $\alpha$ -SMA), type I collagen (Col-I), desmin, and glial fibrillary acidic protein (GFAP),<sup>7,8</sup> cholesterol metabolism, induction of autophagy, endoplasmic reticulum stress, and oxidative stresses.<sup>4</sup>

Integrins and focal adhesion (FA) proteins complex are mechanotransducers and mechanosensors. Indeed, these proteins can act with the cell-cell and cell-ECM interactions through cytoskeleton, importantly participating in the initiation, maintenance, and resolve of fibrosis. Moreover, integrins are capable to connect the cells to ECM proteins, conducting a positional and mechanical indication from the ECM to inside the cell, affecting cell adhesion, migration, and proliferation.<sup>9</sup>

Caveolae are a subgroup of lipid rafts enriched in cholesterol and sphingolipids. Classically, these organelles are described as invaginations of plasma membrane or "little caves" of 60 to 80 nm.<sup>10</sup> These structures can act as mechanic sensors that react to plasma membrane variations. Most importantly, caveolae regulate cholesterol homeostasis and cell physiology as a platform signaling for cell proliferation, migration, and endocytosis.<sup>11,12</sup>

Caveolin-1 (Cav-1), a 22 kDa transmembrane scaffolding protein, is an essential regulator of caveolae present in all plasma membranes and it is indispensable for its formation.<sup>13</sup> Cav-1 and caveolae are both involved in fundamental cellular processes such as endocytosis, transcytosis, signaling pathway transduction, lipid metabolism regulation, and mechanosensors.<sup>1</sup> Many studies demonstrated the importance of cholesterol transport by Cav-1 to membranes, showing a critical role of this protein to membrane homeostasis and organelles functions.<sup>14</sup>

Cav-1 exerts an important hepatic functions through the balance of lipid homeostasis,<sup>1</sup> tissue repair homeostasis, liver fibrosis,<sup>15</sup> and regeneration.<sup>1</sup> It was already described that Cav-1 is increased in both sinusoidal endothelial cells and HSC of cirrhotic livers. This fact was suggested to be related to the portal hypertension that accompanies liver fibrosis.<sup>16,17</sup> Another study demonstrated that Cav-1 protein and messenger RNA increase

in HSC after hepatic damage.<sup>6</sup> Importantly, in physiological and pathophysiological conditions, Cav-1 regulates the homeostasis of lipids and mitochondrial function, appearing as a key sensor protein in the liver tissue. In addition, the overexpression of Cav-1 in cirrhosis condition is related to a defense mechanism that raises the redox status by decreasing nitric oxide (NO) and reactive species of nitrogen production.<sup>1</sup>

GRX cell line is an activated HSC model that was isolated from a hepatic fiber granuloma produced by infection of *Schistosoma mansoni* in C3H/HeN mice.<sup>18</sup> In addition, GRX can be driven to manifest HSC quiescent-like phenotype by treatment with  $\beta$ -carotene, retinol, indomethacin, capsaicin, and lycopene; or to express the HSC activated-like phenotype by stimuli of proinflammatory cytokines. In summary, GRX cell line is an excellent tool for liver fibrosis study.<sup>19-27</sup> Here, we show that exogenous expression of Cav-1 can modify the morphology and metabolism of GRX cells, thus reinforcing its important role in HSC activation. Because Cav-1 has been considered as an attractive strategy for therapeutic design against chronic liver diseases, the GRX<sup>EGFP-Cav1</sup> may be a first-rate tool to focus study Cav-1 as molecular marker of HSC activation.

## 2 | MATERIALS AND METHODS

### 2.1 | Cell culture

The GRX cell line was established by Borojevic et al<sup>18</sup> and kindly provided by the Cell Bank of Rio de Janeiro (HUCFF, UFRJ, RJ, Brazil). Cells were routinely maintained in Dulbecco's modified Eagle's medium (DMEM; Invitrogen, Carlsbad, CA) supplemented with 5% FBS and 2 g/L HEPES buffer, gentamicin 50  $\mu$ g/mL, fungizone 250  $\mu$ g/mL, pH 7.4, at 37°C and 5% CO<sub>2</sub>. All culture reagents were purchased from Sigma-Aldrich.

### 2.2 | Preparation of stable GRX<sup>EGFP-Cav1</sup> cell line

To establish the GRX<sup>EGFP-Cav1</sup> cell line that constitutively overexpresses caveolin-1, we used pCav1EGFP (kindly provided by Dr J. Daniotti, Cordoba University, Argentina) cloned into the recombinant plasmid pcDNA3.1TOPO (Invitrogen) and transformed into through thermal shock. Plasmids were purified using the PureLink Quick Plasmid Miniprep kit (Qiagen). The recombinant plasmid pCav1EGFP (Amp<sup>R</sup>) was transfected into GRX cells at 50% confluence with 2  $\mu$ L of Lipofectamine<sup>TM</sup> (Invitrogen) and 0.3 ng of pCav1EGFP. After 72 hours, transfected cells were selected by addition of 1000  $\mu$ g/mL Geneticin 418 (G418; Sigma-Aldrich) to the culture medium for 4 weeks

and then reduced to 500  $\mu\text{g}/\text{mL}$ . pCI-neo:EGFP (pCI-neo Mammalian Expression Vector; Promega) that expresses EGFP was used as the control plasmid.

### 2.3 | Quantitative real-time reverse transcription polymerase chain reaction

Total RNA (from  $10^6$  cells) was extracted using TRIzol Reagent (Invitrogen) and was reverse-transcribed with SuperScript-II (Invitrogen). RNA expression levels were quantified using SYBR Green on StepOne Plus real-time cyler (Applied-Biosystems, Grand Island, NY) Samples were analyzed using the  $\Delta\Delta C_t$  method<sup>28</sup> with the  $C_t$  values relative to the housekeeping gene  $\beta$ -actin. Gene sequence information was collected from free-internet databases ([www.ensembl.org](http://www.ensembl.org) and <https://www.ncbi.nlm.nih.gov/refseq/>) and used to design specific primers for CAV-1 Forward- 5' GCACACCAAGGAGATTGACC 3', Reverse- 5' GACAACAAGCGGTAAAACCAA3' and  $\beta$ -Actin Forward-5' TATGCCAACACAGTGCTGTCTGG 3' Reverse- 5' TACTCCTGCTTGCTGATCCACAT 3' using a freely available software from Integrated DNA Technologies ([www.idtdna.com](http://www.idtdna.com)).<sup>29</sup>

### 2.4 | Immunoblotting

Protein expression of GRX and GRX<sup>EGFP-Cav1</sup> was detected by Western blot analysis. Cells were lysed in Tris-HCl buffer (pH 6.8) with 2% SDS, 10% glycerol, and 2- $\beta$ -Mercaptoethanol. Equal amounts of protein previously measured according to Peterson<sup>30</sup> were loaded into 10% sodium dodecyl sulfate polyacrylamide gel electrophoresis, transferred into nitrocellulose membranes (Hybond ECL Nitrocellulose Membrane, Amersham), and immunoblotted with the appropriate antibodies. Primary antibodies used were anti-Cav-1 (1:500, SC-53564; Santa Cruz) and anti- $\beta$ -actin (1:500, SC-47778; Santa Cruz). Secondary antibodies used were horseradish peroxidase conjugated antirabbit or anti-mouse-IgG antibodies (1:1000; both from Bio Rad, CA). Proteins blots were detected by chemiluminescence (ECL detection system; Amersham Pharmacia, UK) using Image Quant LAS 4000 (GE Healthcare Chicago). Band intensities were quantified by densitometry using Alpha Easy FC software (version 6.0.0; Genetic Technology Inc., Miami, FL).

### 2.5 | Flow cytometry

For cell counting, GRX and GRX<sup>EGFP-Cav1</sup> were seeded at the density of  $2.5 \times 10^4$  cells/cm<sup>2</sup>. After 24, 48, and 72 hours of culture, cells were trypsinized and suspended in 200  $\mu\text{L}$  of phosphate buffered saline (PBS). Population doublings were defined according to  $\text{PD} = \log N(t) - \log(N(t_0))/\log 2$ , where  $N(t)$  is the number of cells per well at time of

passage, and  $N(t_0)$  is the number of cells seeded at the previous passage.<sup>31</sup> For morphological analysis, the size and cytoplasmic complexity of GRX and GRX<sup>EGFP-Cav1</sup> cells were analyzed using the forward scatter and the side scatter) parameters, respectively. Cell cycle phase progression was analyzed after 48 hours of culture. A total of  $3 \times 10^5$  cells was incubated with cell cycle buffer (3.5 mM de trisodium citrate, 0.5 mM Tris, with 0.05% nonidet), RNase (10 mg/ml) and the DNA was stained with propidium iodide (50  $\mu\text{g}/\text{mL}$ ) for 15 minutes.

Endocytosis capacity of GRX and GRX<sup>EGFP-Cav1</sup> was determined according to Lee et al<sup>32</sup> using red Fluospheres<sup>®</sup> (Fluorescent microspheres; Molecular Probes). Briefly, cells were incubated in a ratio of 1:100 cell/microspheres for 4, 8, and 16 hours. Cells were washed two times with PBS, trypsinized, fixed with 4% paraformaldehyde, and submitted to flow cytometry.

The lysosome quantification was performed through staining cells with Lysotracker Red DND 99 (LysRed) (Invitrogen). Briefly, cells were cultured in 12-well plates, trypsinized and incubated for 30 minutes with LysRed.

All data was acquired with a FACS Calibur cytometry system (FACS Calibur; BD Bioscience, Mountain View, CA) and Cell Quest software (BD Bioscience). Data obtained (20.000 events) was analyzed with FCS Express 4 Software (De Novo Software, Los Angeles, CA).

### 2.6 | Sulphorhodamine B assay

To assess adhesion and proliferation properties, sulphorhodamine B assay was performed.<sup>33</sup> In short, GRX and GRX<sup>EGFP-Cav1</sup> were seeded at  $1 \times 10^4$  cells/cm<sup>2</sup> into 96-well plates and  $2.5 \times 10^4$  cells/cm<sup>2</sup> into 24-well plates. Cell adhesion and proliferation were assessed after 2, 4, and 6 hours for adhesion experiments and 24, 48, and 72 hours for proliferation assay, respectively. Absorbance was measured in a spectrophotometer (Spectra Max M5; Molecular Devices, Sunnyvale, CA) at 560 nm.

### 2.7 | Cholesterol measurement

Free cholesterol content of cells was measured by Amplex Red Cholesterol Assay Kit (Invitrogen) according to the manufacturer's instructions. To measured free cholesterol, cholesterol esterase was omitted from the assay. The values obtained from a cholesterol standard curve were normalized by protein content.

### 2.8 | Microscopy analyses

#### 2.8.1 | Phase contrast microscopy

Cell morphology, transwell cell migration, and wound healing capacity of GRX and GRX<sup>EGFP-Cav1</sup> were analyzed

by phase contrast microscopy using a Nikon Eclipse TE300 inverted microscope. Images were acquired using a Nikon Digital Camera DXM1200C (Düsseldorf, Germany).

### 2.8.2 | Transwell cell migration assay

To test cell migration, transwell migration assay using transparent PET membrane 24 well 8.0  $\mu\text{m}$  pore size according manufactures protocol (ref 353097; Falcon, Corning, NY) was performed. Briefly, cells were plated in transwell chambers at density of  $2 \times 10^4$  cells/cm<sup>2</sup> using serum free DMEM. A total of 700  $\mu\text{L}$  of 10% FBS DMEM was added to the lower chamber and cells were maintained at 37°C and 5% CO<sub>2</sub>. For the migration test, cells were fixed after 16 hours and 22 hours with 4% paraformaldehyde for 15 minutes and then stained with 1% toluidine Blue O (Sigma) for 5 minutes. Cells that migrated were photographed in six randomly selected fields for each membrane in triplicate and counted using the ImageJ software (National Institute of Health, Rock Ville Pike, Bethesda, MD).

### 2.8.3 | Wound-healing cell migration assay

For analyzing cell migration, we followed standard methods with modifications.<sup>34,35</sup> Briefly, GRX and GRX<sup>EGFP-Cav1</sup> were seeded into 24 well and cultured until reach 80% of confluence. After, cells were scratched with a micropipette tip and images were captured at 0, 6, and 24 hours later.

### 2.8.4 | Laser-scanning confocal microscopy

Expression and localization of Cav-1, Col-1,  $\alpha\text{SMA}$ , GFAP,  $\beta 1$  integrin and paxillin were assessed by fluorescence labeling. Lysosomal function and endocytosis were respectively analyzed by LysRed staining and microspheres uptake FluoSpheres®. For all experiments, GRX and GRX<sup>EGFP-Cav1</sup> cells were cultured in appropriate glass bottom culture plates (CELLview Glass bottom plates; GreinerBioone).

For immunofluorescence labeling, cells were fixed with 4% paraformaldehyde before incubating with the primary antibodies (1:500) Cav-1, collagen-I,  $\alpha\text{SMA}$ ,  $\beta 1$  Integrin (sc53564, sc8784, sc1615, sc8978, respectively; all from Santa Cruz Biotechnology, Dalas), GFAP (ZO334, from DAKO, Glostrup, Denmark), and paxillin (610051; BD Biosciences, San Jose, CA). Sequentially, cells were incubated with the secondary antibody (1:1000) Alexa-Fluor 408, AlexaFluor 555, or AlexaFluor 647

(Invitrogen). The fluorescent dye Hoechst 33342 (H1398; Invitrogen) was used for labeling cell nuclei.

LysRed staining were performed as in accordance to the manufacturer's instructions. To visualize microspheres uptake cells were incubated by 8 hours with 1:100 cells/microspheres according.<sup>32</sup> To contrast, actin cytoskeleton was stained with Phalloidin - AlexaFluor 488 (Invitrogen) and cell nuclei with Hoechst 33342 (Invitrogen). In this experiment, images underwent a three-dimensional reconstruction of the sweep on the Z axis. For actin cytoskeleton analysis, cells were stained with Actin Red™ 555 (R37112; Invitrogen) for 30 minutes in accordance to the manufacturer's instructions

All images were collected using Olympus FV1000 laser-scanning confocal microscope. Ten single confocal sections of 0.7  $\mu\text{M}$  were taken parallel to the bottom plates (xy sections). All experiments were performed at least four times for each sample. Images from six random fields were acquired, deconvolved using the Interactive 3D plugin and cell fluorescence intensity was analyzed using the software ImageJ (National Institute of Health, Rock Ville Pike, Bethesda, MD, EUA). Colocalization analysis was performed using intensity correlation analysis plugin of ImageJ.<sup>36</sup>

### 2.8.5 | Electron microscopy

Cells were fixed in 4% paraformaldehyde plus 2.5% glutaraldehyde in 0.1 M phosphate buffer (PB) at room temperature. Afterwards, they were washed in PB and fixed in 1% osmium tetroxide, OsO<sub>4</sub> (Sigma) in PB, pH 7.4 for 1 hour at room temperature. They were washed again with PB and then gradually dehydrated with acetone (Merck) and soaked in epon resin. Polymerization was carried out for 48 hours at 60°C. Semi-thin sections (1  $\mu\text{m}$ ) were made in ultramicrotome (Leica EM UC7) and stained with 1% toluidine blue. Ultrafine cuts were obtained in an ultramicrotome for the assembly of copper grids (200 mesh). Samples were counterstained with 1% uranyl acetate (Merck) and then with 1% lead citrate (Merck). Cell morphology, autophagosomes, and autolysosomes were observed using TEM at an 80-kV acceleration voltage (JEM 1200; EXII, Japan).

## 2.9 | Statistical analysis

Data were obtained at least from three independent experiments done in triplicate and expressed as mean values  $\pm$  SD. Statistical comparisons were carried out by one- or two-way analysis of varianc followed by Bonferroni's post hoc test. When necessary, Student t-test

was used. Statistical significance was accepted at  $P < .05$ . All analyses and graphics were performed using the statistical software GraphPad Prism 6 for Windows (version 6; GraphPad Software Inc., Sa Diego).

### 3 | RESULTS

#### 3.1 | Caveolin-1 expression in the GRX<sup>EGFP-Cav1</sup> activation

GRX<sup>EGFP-Cav1</sup> expresses around 83% more Cav-1 when compared to nontransfected GRX and the green fluorescence form EGFP colocalizes with anti-Cav-1 antibody in red, revealing Pearson coefficient of  $0.82 \pm 0.02$ , as expected (Figure S1). To ensure that Cav-1 may be responsible by all changes in GRX<sup>EGFP-Cav1</sup>, we tested the GRX cells transfected with a plasmid that expresses only the EGFP, GRX<sup>EGFPpCineo</sup> (pCI-neo mammalian expression vector; Promega). Thus, we found that EGFP did not interfere in cell proliferation, cell adhesion after 2 hours, Cav-1 expression, lysosomal function and GRX<sup>EGFPpCineo</sup> cell ultrastructure (Figure S2). Activation of HSC, transdifferentiation of quiescent into activated myofibroblasts, is well defined as a primary driver of liver fibrosis. The expression of  $\alpha$ -SMA, Col-I, GFAP, as well as the changes on the cholesterol metabolism and the autophagy rate by lysosomal stimulation, are reliably markers that are generally used to assess HSC activation.<sup>4</sup> Therefore, we investigated the activation state of GRX and GRX<sup>EGFP-Cav1</sup> through analyzing these classical parameters. In all immunofluorescence labeling for  $\alpha$ -SMA, Col-I and GFAP, it was noticed an increase on the intensity of fluorescence (IF) in GRX<sup>EGFP-Cav1</sup> in comparison to GRX cells (Figure 1A).

Caveolae may show a homogeneous distribution on the plasma membrane with association of actin stress fibers.<sup>12</sup> In a previous work, our group showed that the treatment with proinflammatory cytokines induce the GRX cells to a more activated state with a reorganization of actin cytoskeleton.<sup>27</sup> GRX cells present a typical myofibroblast phenotype grow in a “hills and valleys” model, characteristic of the smooth muscle cells lineages, had low contact inhibition and have a well-organized stress-fibers.<sup>22</sup> On the other hand, GRX<sup>EGFP-Cav1</sup> cells grow into small clusters composed of several cells climbing over each other. In addition, labeling with Actin Red 555 in GRX<sup>EGFP-Cav1</sup> showed that stress fibers were reduce in length with a granular actin perinuclear zone. An extensive dense peripheral actin-rich border and distant large focal adhesions at the end of long pseudopodia (Figure 1B). In concordance with previously description for the activation of GRX,<sup>27</sup> these results reinforce the hypothesis that the cell-cell adhesion was

stronger than cell-substrate adhesion. In addition, the IF for Actin Red 555 was higher in GRX<sup>EGFP-Cav1</sup>, thus suggesting an interconnection between the increased Cav-1 expression and the amount/structure of the actin cytoskeleton (Figure 1B). We further examine whether expression of Cav-1 is implicated in cholesterol metabolism by Amplex Red method and it was found an increase of free cholesterol in GRX<sup>EGFP-Cav1</sup> compared to GRX (Figure 1C). Altogether, these results are in accordance to the previous description of GRX and/or HSC activation.

#### 3.2 | Cav-1 in cell migration

Cav-1 and caveolae play an important role in cell migration.<sup>37</sup> Therefore, we conducted the transwell experiments to view chemotaxis attractive interaction in response to the increased expression of Cav-1. GRX<sup>EGFP-Cav1</sup> presented an increased capacity on migrating toward the chemo-attractant after 16 and 22 hours in comparison to the GRX. Interestingly, GRX<sup>EGFP-Cav1</sup> remained in clusters when passing through the transwell, showing strong attraction between cells produced by the activation process, suggesting enhances polarity and collective cell movement migration (Figure 2A).

In wound healing experiment at time 0 hours GRX<sup>EGFP-Cav1</sup> opened a larger wound. Curiously, cells detached from the substrate as a layer and these cells adhere again on the edges of wound (Figure 2B black arrow). On the other hand, GRX detached from the substrate individually. These phenomena are very interesting because GRX<sup>EGFP-Cav1</sup> showed an enhanced mechanosensory, surface tension, and cell-cell affinity to continually attached to others.<sup>38</sup> Curiously, at time 6 hours, migration pattern of both cell lines is different. GRX expanded pseudopodium-like projections into the free space and have a cell single migration. On the other hand, GRX<sup>EGFP-Cav1</sup> cells showed a collective migration pattern, suggesting a lamellipodial crawling movement (Figure 2B white arrow). After, 24 hours both cells lines closed the wound. Collectively, these results demonstrated that Cav-1 accelerated transwell migration in chemo-attractant conditions, and in the wound healing experiment demonstrated a different pattern of migration for both cell lines, higher superficial tension and cell-cell affinity in GRX<sup>EGFP-Cav1</sup> (Figure 2B).

#### 3.3 | Effects of caveolin-1 expression on cell cycle

Although the proliferation curve of transfected cells appears to indicate a higher rate of proliferation compared to GRX cells, the calculation of population doubling

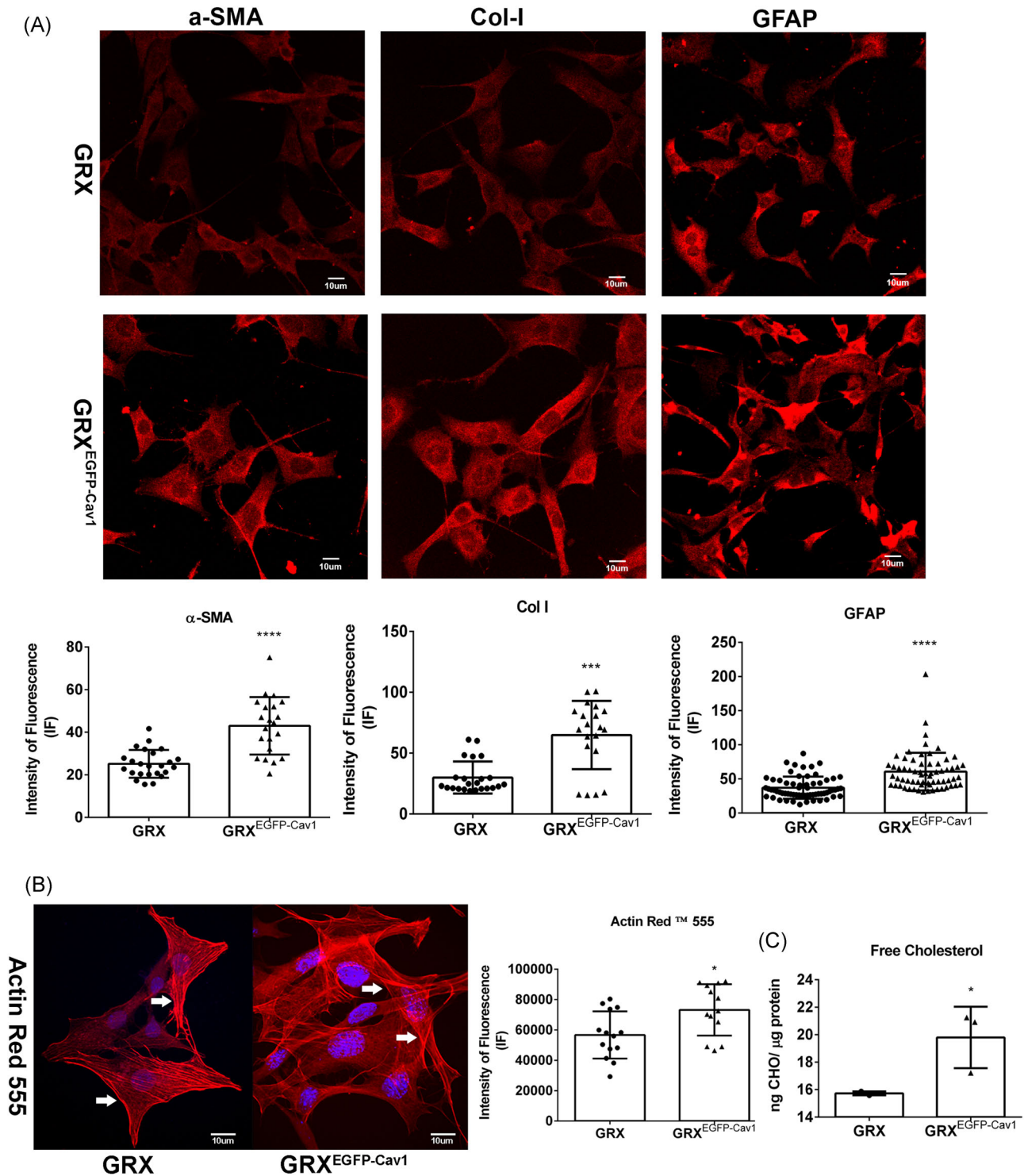


**FIGURE 1** Cav-1 expression in the GRX and GRX<sup>EGFP-Cav1</sup> activation. Representative confocal images of GRX and GRX<sup>EGFP-Cav1</sup>. A, Cells were immunolabelled for α-SMA, Col-I and GFAP with Alexa Fluor 555 secondary antibody. Scale Bar 10 μm. B, Cells were stained with TRITC Rhodamine phalloidin Scale Bar 10 μm. Intensity of fluorescence (IF) were quantified by ImageJ. C, Quantification of free cholesterol was performed by Amplex Red. Cellular IF means ± SD were presented. \**P* < .05; \*\*\* *P* < .001; \*\*\*\**P* < .0001. α-SMA, alpha-smooth muscle actin; caveolin-1, Cav-1; Col-I, collagen I

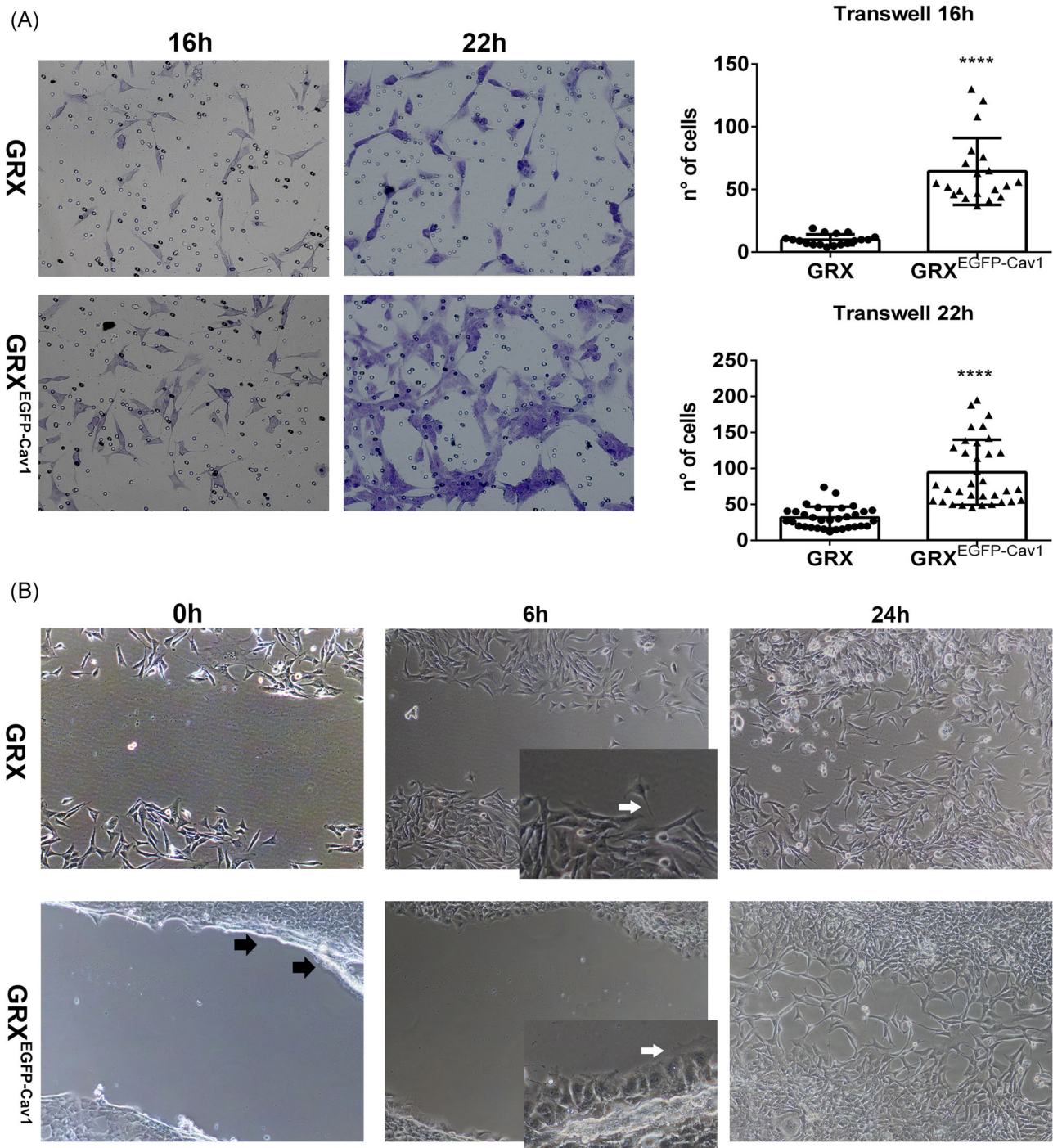


**FIGURE 2** Cav-1 in Directional Migration. A, Representative images of GRX and GRX<sup>EGFP-Cav1</sup> cell in transwell migration at 16 and 22 hours. Cells were staining with Toluidine Blue O, (total magnification 100×). Pores of the membrane are visible as spots. Quantification of cells migration in 16 and 22 hours was performed by Image J. B, Representative images of GRX and GRX<sup>EGFP-Cav1</sup> at 0, 6, and 24 hours after monolayer injury. In 0 hours, GRX<sup>EGFP-Cav1</sup> showed a larger wound and layer of detached cells attached again on the edges (black arrow). After 6 hours migration pattern was different in both cell lines. In zoom, detailed GRX demonstrated a single cell pattern of migration (white arrow) whereas GRX<sup>EGFP-Cav1</sup> demonstrated a collective pattern of migration. In 24 hours, both cell lines closed wound. \*\*\*\**P* < .0001. Caveolin-1, Cav-1

(CPD) and growth coefficient did not differ between the two cell lines (Figure 3A). This can be explained by the comparison between the adhesion proprieties of GRX cells and GRX<sup>EGFP-Cav1</sup>. GRX<sup>EGFP-Cav1</sup> presented an increased

cell adhesion, when evaluated in 2 hours, and this pattern was maintained over 4 and 6 hours after plating (Figure 3B). Despite the increased number of adhered cells, GRX<sup>EGFP-Cav1</sup> exhibited a distinct adhesion pattern since

cells remained rounded for at least 2 hours after plating. In contrast, 2 hours after plating, GRX cells already have well-formed cytoplasmic processes, demonstrating its cell spreading, traction force magnitude, cytoskeleton remodeling, and possibly more hydrophilic proprieties by substrate (Figure 3B). Thus, cell cycle progression in GRX and GRX<sup>EGFP-Cav1</sup> were analyzed by flow cytometer. Significantly, GRX<sup>EGFP-Cav1</sup> showed a reduction in percent of cells in G0/G1 phase and an increase in percent of cells in the S phase, but number of cells in G2/M was similar in both cell lines (Figure 3C). Caveolin regulate cell cycle and tumor progression in some cases.<sup>13</sup>

### 3.4 | Effects of caveolin-1 expression in adhesion complex

Integrins communicate positional and mechanical signals from the ECM to the extracellular milieu, modulating important cell function such as adhesion, migration, and proliferation.  $\beta 1$  integrin and paxillin are adhesions proteins connected with Cav-1 and ECM.<sup>39,40</sup> To investigate if these proteins are involved in the aforementioned adhesion pattern, we evaluated their expression by measurement of IF in GRX and GRX<sup>EGFP-Cav1</sup>, seeking for the potential proteins colocalizations. As expected, the IF of both proteins was increased in response to exogenous expression of Cav-1 (Figure 4A and 4B). Colocalization

between  $\beta 1$  integrin and Cav-1 in GRX and GRX<sup>EGFP-Cav1</sup> was demonstrated by the analysis of images presented in Figure 4A. Furthermore, the  $\beta 1$  integrin/Cav-1 colocalization was clearly enhanced in GRX<sup>EGFP-Cav1</sup>. Moreover,  $\beta 1$  integrin and paxillin are distributed and colocalized throughout all cell cytoplasm (Figure 4B), thus indicating a strong interaction between these proteins. Indeed, immunofluorescence of paxillin showed more FA sites and increased of IF in GRX<sup>EGFP-Cav1</sup>, which may implicate in the recruitment of many structural and regulatory proteins to the cell adhesion sites. In summary, these results support the evidence that exogenous expression of Cav-1 is capable to modify the cell cycle and to change the cell adhesion pattern.

### 3.5 | Impact of Cav-1 expression on cell morphology and endocytosis flux

Caveolin proteins are best known for their facilitations of the formation of plasma membrane caveolae.<sup>13</sup> To examine the effect of exogenous expression of Cav-1 on GRX cell line, we analyzed cellular ultrastructure by TEM (Figure 5A). Among the observed differences between transfected and nontransfected cells, the most remarkable fact was the presence of autophagosome-like structures and autophagolysosomes (AL). Also, we visualized a notable of clumping caveolae (white circles)

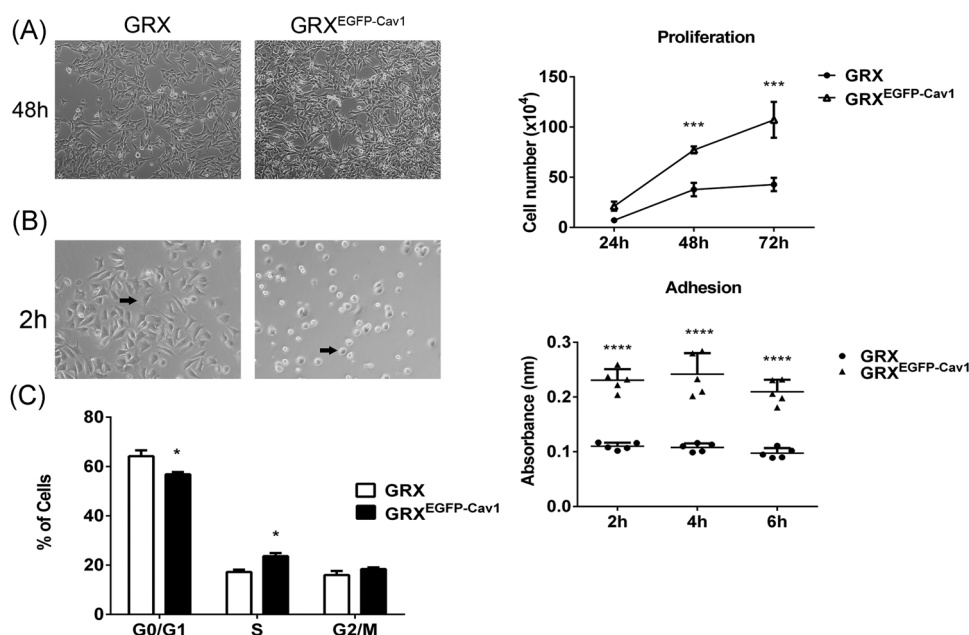


**FIGURE 3** Effects of Caveolin-1 on cell proliferation and adhesion. A, Images from phase-contrast microscopy on cell morphology on 48 hours and cell proliferation after 24, 48, and 72 hours of culture. For GRX and GRX<sup>EGFP-Cav1</sup> calculation of population doubling (CPD) revealed a growth coefficient of 0.835 and 0.818 and a duplication time of 20 and 19 hours. B, Images from phase-contrast microscopy in 2 hours after plating (black arrows) and cell adhesion measured by sulphorhodamin B. assay after 2, 4, and 6 hours. Magnification of 200 $\times$ . C, Cell cycle was analyzed by flow cytometry. \* $P < .05$ ; \*\*\* $P < .001$ ; \*\*\*\* $P < .0001$

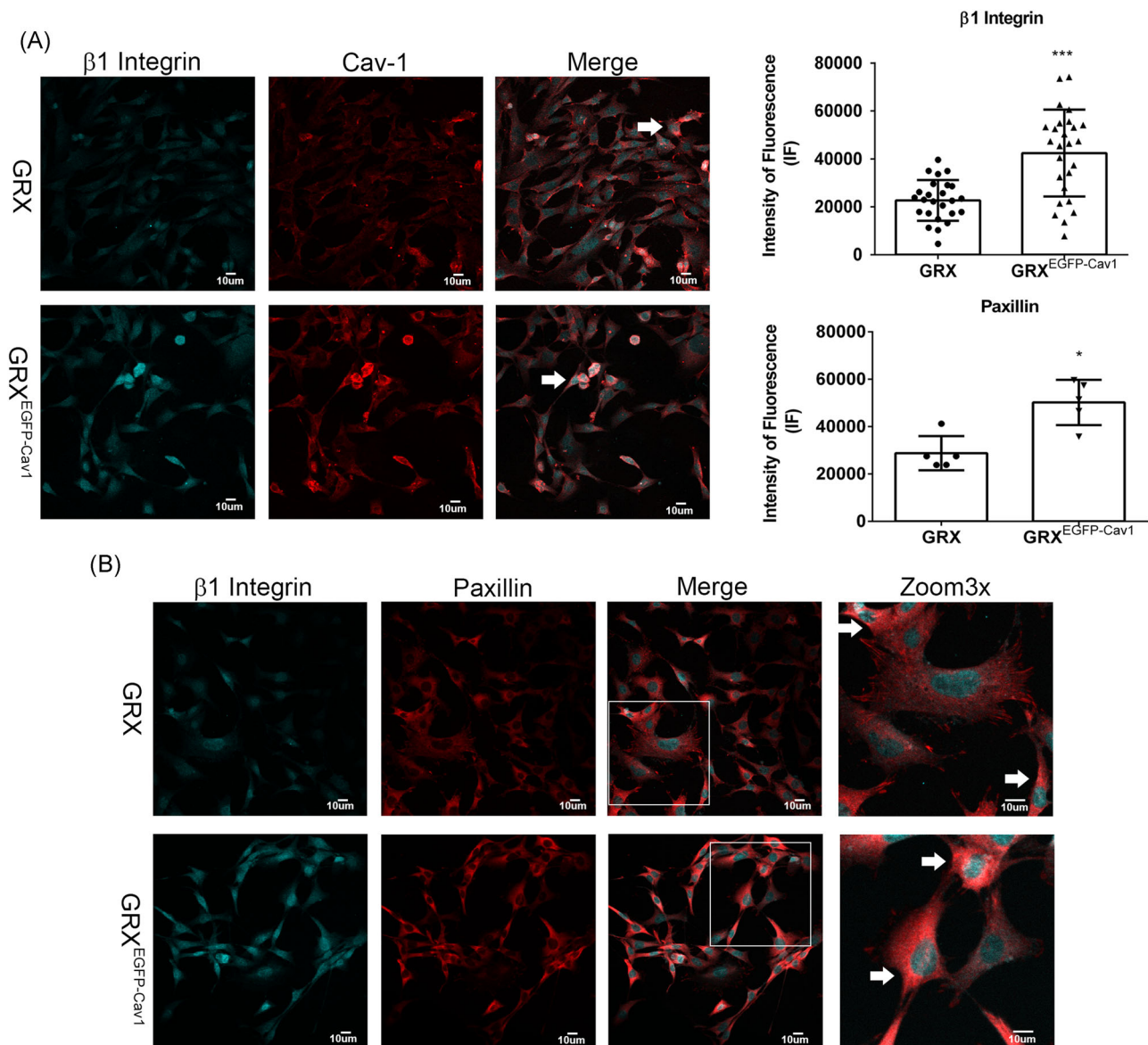


**FIGURE 4** Effects of Cav-1 in  $\beta 1$  Integrin and paxillin expression. A, B, Cells were immunolabelled for  $\beta 1$ -integrin, caveolin-1 and paxillin with monoclonal anti-( $\beta 1$  integrin), anti-(Cav-1) and anti-(paxillin) antibodies, with Alexa Fluor 405 (cyan-blue) and 555 secondary antibodies, thus examined by confocal microscopy. Colocalization were indicated by a white arrow. Scale bars, 10  $\mu\text{m}$ . The  $\beta 1$  Integrin and paxillin expression was evaluated by measuring the intensity of fluorescence (IF) using Image J. Values are means  $\pm$  SD from random fields as described in Material and Methods. \* $P < .05$ ; \*\*\* $P < .001$ . Caveolin-1, Cav-1

in transfected cells (Figure 5A). Likewise, the data of TEM (Figure 5A) showed an endoplasmic reticulum (ER) dilated in GRX<sup>EGFP-Cav1</sup> when compared with GRX, thus suggesting ER stress. In addition, HSC activation is triggered by ER stress and autophagy, producing thus fatty acids from cleavage of retinyl esters.<sup>4</sup> These results indicated that exogenous Cav-1 promoted a great change in the cytoplasm of GRX<sup>EGFP-Cav1</sup>, which may be responsible for the greater granularity shown by these cells in the morphological analysis by flow cytometry (Figure S1F-G).

Because TEM analysis revealed presence of autophagosome-like structures and AL, we examined whether

Cav-1 expression affects lysosomal function by evaluating LysRed stained cells. Notably, there was a significant increase in LysRed in GRX<sup>EGFP-Cav1</sup> when comparing to GRX, indicating enhanced acidification of lysosomes (Figure 5B). Autophagy is a dynamic process constituted by a succession of steps leading to the formation of autophagosomes. After fusion with lysosomes, the cargo material is degraded.<sup>41</sup>

Since TEM analysis revealed many caveolae (Figure 5A), we evaluated the endocytosis capacity of GRX and GRX<sup>EGFP-Cav1</sup> cells using FluoSpheres<sup>®</sup> by flow cytometry. Endocytosis capacity was increased in GRX<sup>EGFP-Cav1</sup> cells after 8 hours of cell incubation, reaching a plateau

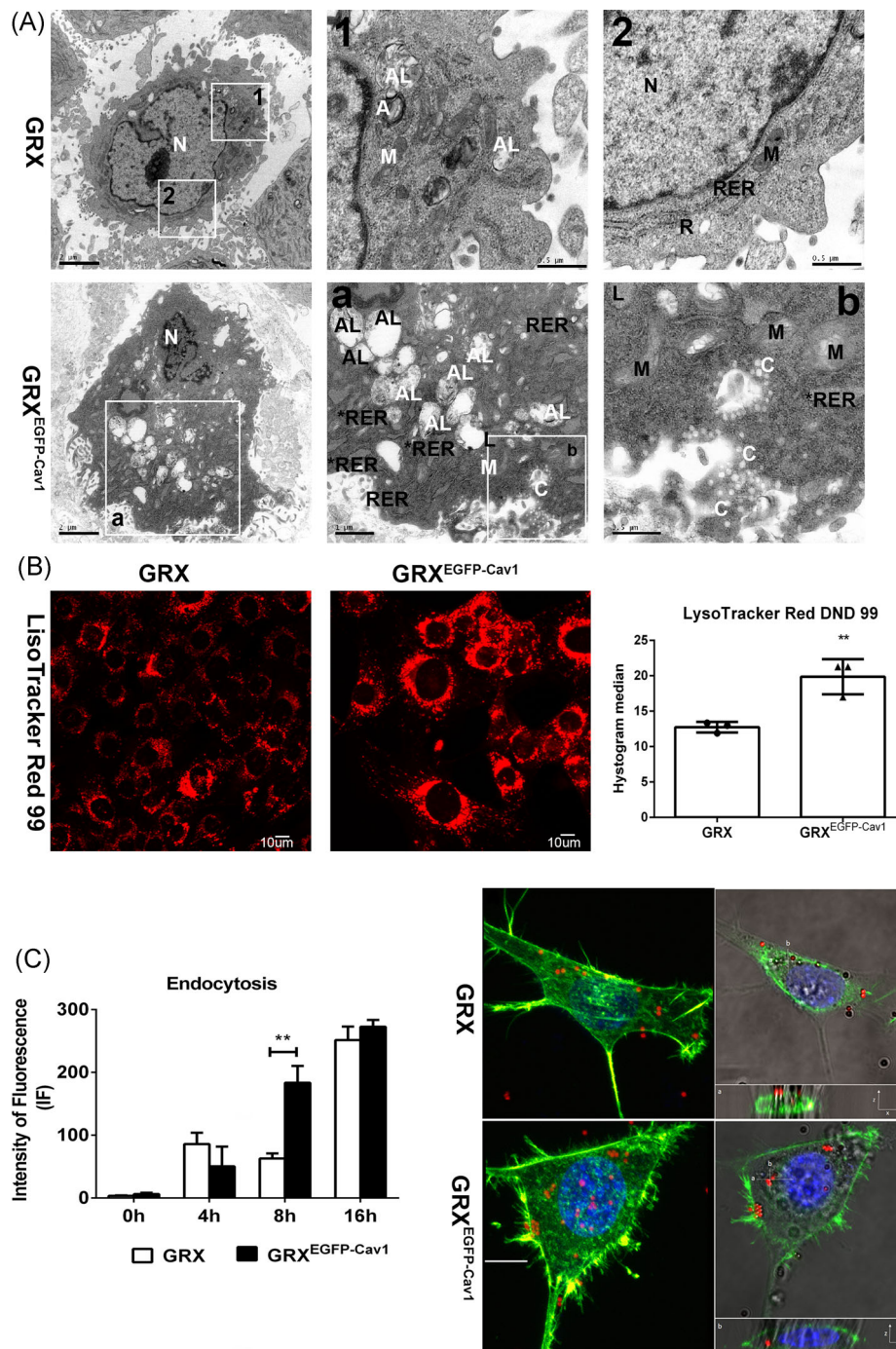


**FIGURE 5** Impact of Cav-1 expression on cell morphology and endocytosis flux: A, Ultrastructural analysis assessed by TEM: Nucleus (N), mitochondria (M), autophagolysosomes (AL), mature autophagosome (A), rough endoplasmic reticulum (RER), dilated RER (RER\*), caveolae (white C), lysosome (L). Scale bars, 2, 1, and 0.5  $\mu\text{m}$ . B, Representative images of lysosomal function after staining with LysRed. C, 3D reconstruction revealed the FluoSpheres® inside GRX and GRX<sup>EGFP-Cav1</sup>. Images represent a 3D project and the orthogonal view of GRX and GRX<sup>EGFP-Cav1</sup> after incubation with FluoSpheres®, displayed using Image J software. An x,z section was demonstrated at the bottom and y,z at the right. Scale bars, 10  $\mu\text{m}$ . \*\*  $P < .001$ . Caveolin-1, Cav-1; 3D, three-dimensional; TEM, transmission electron microscopy

after 16 hours. Phalloidin counterstaining for the three-dimensional imaging reconstruction confirmed that the FluoSpheres® were inside the cells (Figure 5C). These data indicated that exogenous expression of Cav-1 was able to accelerate the endocytosis flux in GRX<sup>EGFP-Cav1</sup> cells.

## 4 | DISCUSSION

Our group<sup>22,25</sup> has demonstrated that GRX has GFAP and Col-I expression and we show that exogenous expression of Cav-1 increases the expression of GFAP, Col-I,  $\alpha$ -SMA

and the amount of free cholesterol in GRX<sup>EGFP-Cav1</sup> cell line than in GRX. HSC have an important typical transcriptomic profile that expresses a variation of genes and proteins that differentiate these cells from others liver cells. There are well-known molecular markers for myofibroblast differentiation like the increased content of  $\alpha$ -SMA and Col-1.<sup>4</sup> In addition, GFAP is expressed *in vivo* in HSC<sup>7</sup> and is increased in the chronic liver fibrotic response.<sup>4,8</sup> Another characteristic involved in HSC activation is enhances of free cholesterol content. It is important to note that dilated or stressed ER is associated to the fibrogenic gene expression in HSC and to the increased autophagy during HSC activation. Indeed, ER is the cellular site of cholesterol synthesis. Cav-1 binds to cholesterol and regulates the cholesterol trafficking – import and export – to and between the plasma membrane and other cellular sites.<sup>4,13</sup> Unlike in most organs, such as heart, lung, and kidney, Cav-1 operates as a pro-fibrotic role in hepatic tissue. Cav-1 binds to cholesterol and its levels are increased in cirrhosis, showing an interdependence of two molecules in the pathophysiology of liver diseases.<sup>42</sup>

Cav-1 was linked to proliferation and cell cycle in several studies.<sup>13</sup> Furthermore, exogenous expression of Cav-1 did not change the CPD; however, modified cell cycle through enhancing the percentual number of cells at phase S and decreasing at phase G0/G1. Indeed, Cav-1 is thought to regulate cell cycle and tumor progression through modulating of signaling by the Ras/MAPK pathway. This fact could indicate that soluble Cav-1 is carried into the nucleus, regulating gene expression. In the nucleus, Cav-1 can bind to promoters and can down-regulate the expression of genes responsible for controlling of cell proliferation, such as cyclin D1 and folate receptor.<sup>13</sup>

Our findings support the notion that Cav-1 modulated actin cytoskeleton,  $\beta$ 1 integrin, and paxillin complex by enhancing cell polarization, directional migration, adhesion proprieties, and cell-cell affinity. We showed that exogenous expression of Cav-1 increases the protein content of  $\beta$ 1 integrin, paxillin, and f-actin, which are important FA proteins on promoting the connection between cell cytoskeleton and ECM. In addition, we evaluated the impact of Cav-1 in the cell migration. GRX<sup>EGFP-Cav1</sup> cells presented an accelerated and collective migration toward chemoattractant media and an extended abroad (lamellipodia) migration. On the other hand, GRX cells presented an extended spike-like protrusion (filopodia) and a single cell migration. In the wound healing assay, it was possible to note the formation of FA in both GRX<sup>EGFP-Cav1</sup> and GRX cells. Mechanosensing is when cells transduce the mechanical proprieties to cells-ECM and cell-cell interactions through FA that are linked to actin fibers.<sup>43</sup> Integrins are an important cell adhesion proteins that act in cell-

cell and cell-ECM interactions, and are the first to be activated among FA proteins during wound healing responses.<sup>3,40,43</sup> Indeed,  $\beta$ 1 integrin protein increase is associated with the progression of fibrotic liver diseases.<sup>40</sup> Cav-1 and  $\beta$ 1 integrin have a strong association with adhesion proprieties and migration, remodeling actin cytoskeleton and stabilizing the focal adhesion kinase at FA.<sup>37</sup> How cells collectively adjust their forces and how they sense and transduce the mechanical properties of their neighbors cells are currently under intensive investigation.<sup>43</sup>

In the present study, expression of Cav-1 enhanced the number of caveolae, revealing noticeable changes in cell morphology of GRX<sup>EGFP-Cav1</sup>. Accordingly, GRX<sup>EGFP-Cav1</sup> cells have greater size and cytoplasmic complexity. The appearance of autophagolysosomes in GRX<sup>EGFP-Cav1</sup> was higher and concomitant to the increase of lysosome revealed by the LysRed signal in comparison to GRX. Cav-1 has an extensive membrane distribution in all organelles, including lysosomes. Moreover, autophagy drives HSC activation by generating metabolic homeostasis.<sup>41,44</sup>

In fact, in ours results we demonstrated that GRX<sup>EGFP-Cav1</sup> cells endocytosed more FluorSpheres<sup>®</sup> when compared with GRX. Importantly, Cav-1 and its interactions with actin cytoskeleton and ATP play a pivotal role in the structure, formation, and function of caveolae.<sup>12,13,41,45,46</sup> Although these results may be related to the increase on the caveolae number, it is possible that FluorSpheres<sup>®</sup> uptake can be being driven by both caveolar endocytosis or clathrin-dependent endocytosis.<sup>12,47</sup>

GRX cells represent a heterogeneous population that can be induced to have majority activated or quiescent cells.<sup>20,25,48,49</sup> Here, we showed for the first time that exogenous expression of Cav-1 (GRX<sup>EGFP-Cav1</sup>) induced the majority of the GRX population into an activated-like HSC state. The established cell lines can have a high impact on strategy and comprehension of cellular biology, substantially contributing to novel therapeutic design for liver fibrosis study. Our results suggest that Cav-1 is a new possible candidate for molecular marker of HSC activation. Because Cav-1 is enhanced in the context of pathophysiology, an advantage on establishing a GRX model that expresses increased levels of Cav-1, is the possibility to focus on future pivotal studies and the role of Cav-1 on molecular mechanisms involved in HSC activation at cellular level. In this sense, further studies are indispensable to fully understand possible healing cooperation of Cav-1 in liver fibrosis, when rapid reversal is required. The GRX<sup>EGFP-Cav1</sup> cell line is accessible to be used for research to further understand the pathology and physiopathology of liver fibrosis and its susceptibility to new available medications.

## ACKNOWLEDGMENTS

Mariana Ilha is a recipient of PhD degree fellowship from CNPq (Conselho Nacional de Desenvolvimento Científico e Tecnológico - Brazil). FCR Guma, G Lenz, LA Meira Martins, F Barbe-Tuana and F Rodhen are recipients of a research fellowship from CNPq. The authors thank Dr JL Daniotti for the donation of pCav1EGFP plasmid and Dra. Iduvirges Lourdes Müller for some ideas to this study. This study was supported by CAPES, MCT/CNPq Universal (423712/2016-0), PqG/FAPERGS 1952-2551/13 and PROPESQ-UFRGS.

## CONFLICT OF INTERESTS

The authors declare that there are no conflict of interests.

## AUTHOR CONTRIBUTIONS

Conceived and design the analysis: MI, FG. Collected data: MI, KM, FR, LM, RB. Performed the analysis: MI, FB, LM, FR, FG. Wrote the paper: MI. Contribution to the text writing: LM, GL, FB, FG.

## ORCID

Mariana Ilha  <http://orcid.org/0000-0001-9741-8865>  
 Francieli Rohden  <http://orcid.org/https://orcid.org/0000-0002-9232-7371>  
 Leo Anderson Meira Martins  <http://orcid.org/https://orcid.org/0000-0003-0878-0489>  
 Radovan Borojevic  <http://orcid.org/https://orcid.org/0000-0002-2393-7280>  
 Guido Lenz  <http://orcid.org/https://orcid.org/0000-0003-4077-6316>  
 Florencia Barbé-Tuana  <http://orcid.org/https://orcid.org/0000-0002-5358-3524>  
 Fátima Costa Rodrigues Guma  <http://orcid.org/https://orcid.org/0000-0003-2369-7739>

## REFERENCES

- Fernandez-Rojo MA, Ramm GA. Caveolin-1 function in liver physiology and disease. *Trends Mol Med*. 2016;22:889-904. <https://doi.org/10.1016/j.molmed.2016.08.007>
- Marcellin P, Kutala BK. Liver diseases: a major, neglected global public health problem requiring urgent actions and large-scale screening. *Liver Int*. 2018;38(Suppl 1):2-6. <https://doi.org/10.1111/liv.13682>
- Pellicoro A, Ramachandran P, Iredale JP, Fallowfield JA. Liver fibrosis and repair: immune regulation of wound healing in a solid organ. *Nat Rev Immunol*. 2014;14:181-194. <https://doi.org/10.1038/nri3623>
- Tsuchida T, Friedman SL. Mechanisms of hepatic stellate cell activation. *Nat Rev Gastroenterol Hepatol*. 2017;14:397-411. <https://doi.org/10.1038/nrgastro.2017.38>
- Bataller R, Brenner DA. Liver fibrosis. *J Clin Invest*. 2005;115:209-218. <https://doi.org/10.1172/JCI24282>
- Singh S, Liu S, Rockey DC. Caveolin-1 is upregulated in hepatic stellate cells but not sinusoidal endothelial cells after liver injury. *Tissue Cell*. 2016;48:126-132. <https://doi.org/10.1016/j.tice.2015.12.006>
- Tennakoon AH, Izawa T, Wijesundera KK, et al. Characterization of glial fibrillary acidic protein (GFAP)-expressing hepatic stellate cells and myofibroblasts in thioacetamide (TAA)-induced rat liver injury. *Exp Toxicol Pathol*. 2013;65:1159-1171. <https://doi.org/10.1016/j.etp.2013.05.008>
- Carotti S, Morini S, Corradini SG, et al. Glial fibrillary acidic protein as an early marker of hepatic stellate cell activation in chronic and posttransplant recurrent hepatitis C. *Liver Transpl*. 2008;14:806-814. <https://doi.org/10.1002/lt.21436>
- Schuppan D, Ashfaq-Khan M, Yang AT, Kim YO. Liver fibrosis: direct antifibrotic agents and targeted therapies. *Matrix Biol*. 2018;68-69:435-451. <https://doi.org/10.1016/j.matbio.2018.04.006>
- Wang J, Schilling JM, Niesman IR, et al. Cardioprotective trafficking of caveolin to mitochondria is Gi-protein dependent. *Anesthesiology*. 2014;121:538-548. <https://doi.org/10.1097/ALN.0000000000000295>
- Kovtun O, Tillu VA, Jung W, et al. Structural insights into the organization of the cavin membrane coat complex. *Dev Cell*. 2014;31:405-419. <https://doi.org/10.1016/j.devcel.2014.10.002>
- Parton RG, del Pozo MA. Caveolae as plasma membrane sensors, protectors, and organizers. *Nat Rev Mol Cell Biol*. 2013;14:98-112. <https://doi.org/10.1038/nrm3512>
- Fridolfsson HN, Roth DM, Insel PA, Patel HH. Regulation of intracellular signaling and function by caveolin. *FASEB J*. 2014;28:3823-3831. <https://doi.org/10.1096/fj.14-252320>
- Bosch M, Mari M, Gross SP, Fernandez-Checa JC, Pol A. Mitochondrial cholesterol: a connection between caveolin, metabolism, and disease. *Traffic*. 2011;12:1483-1489. <https://doi.org/10.1111/j.1600-0854.2011.01259.x>
- Gvaramia D, Blaauboer ME, Hanemaaijer R, Everts V. Role of caveolin-1 in fibrotic diseases. *Matrix Biol*. 2013;32:307-315. <https://doi.org/10.1016/j.matbio.2013.03.005>
- Yokomori H, Ando W, Oda M. Caveolin-1 is related to lipid droplet formation in hepatic stellate cells in human liver. *Acta Histochem*. 2019;121:113-118. <https://doi.org/10.1016/j.acthis.2018.10.008>
- Yokomori H, Oda M, Ogi M, Sakai K, Ishii H. Enhanced expression of endothelial nitric oxide synthase and caveolin-1 in human cirrhosis. *Liver*. 2002;22:150-158. [https://doi.org/10.1588\[pil\]](https://doi.org/10.1588[pil])
- Borojevic R, Monteiro AN, Vinhas SA, et al. Establishment of a continuous cell line from fibrotic schistosomal granulomas in mice livers. *In Vitro Cell Dev Biol*. 1985;21:382-390.
- Elias MB, Oliveira FL, Guma FCR, Martucci RB, Borojevic R, Teodoro AJ. Lycopene inhibits hepatic stellate cell activation and modulates cellular lipid storage and signaling. *Food Funct*. 2019;10:1974-1984. <https://doi.org/10.1039/c8fo02369g>
- Guimaraes EL, Franceschi MF, Grivicich I, et al. Relationship between oxidative stress levels and activation state on a hepatic stellate cell line. *Liver Int*. 2006;26:477-485. <https://doi.org/10.1111/j.1478-3231.2006.01245.x>

21. Margis R, Borojevic R. Retinoid-mediated induction of the fat-storing phenotype in a liver connective tissue cell line (GRX). *Biochim Biophys Acta*. 1989;1011:1-5. [https://doi.org/0167-4889\(89\)90069-4](https://doi.org/0167-4889(89)90069-4)[pii].
22. Mermelstein CS, Guma FC, Mello TG, et al. Induction of the lipocyte phenotype in murine hepatic stellate cells: reorganisation of the actin cytoskeleton. *Cell Tissue Res*. 2001;306:75-83.
23. Monteiro AN, Borojevic R. Interaction of human liver connective tissue cells, skin fibroblasts and smooth muscle cells with collagen gels. *Hepatology*. 1987;7:665-671. <https://doi.org/S0270913987000983>[pii]
24. Pinheiro-Margis M, Margis R, Borojevic R. Collagen synthesis in an established liver connective tissue cell line (GRX) during induction of the fat-storing phenotype. *Exp Mol Pathol*. 1992;56:108-118.
25. Borojevic R, Guaragna RM, Margis R, Dutra HS. In vitro induction of the fat-storing phenotype in a liver connective tissue cell line-GRX. *In Vitro Cell Dev Biol*. 1990;26:361-368.
26. Teodoro AJ, Perrone D, Martucci RB, Borojevic R. Lycopene isomerisation and storage in an in vitro model of murine hepatic stellate cells. *Eur J Nutr*. 2009;48:261-268. <https://doi.org/10.1007/s00394-009-0001-6>
27. da Silva FM, Guimaraes EL, Grivicich I, et al. Hepatic stellate cell activation in vitro: cell cycle arrest at G2/M and modification of cell motility. *J Cell Biochem*. 2003;90:387-396. <https://doi.org/10.1002/jcb.10642>
28. Schmittgen TD, Livak KJ. Analyzing real-time PCR data by the comparative C(T) method. *Nat Protoc*. 2008;3:1101-1108.
29. Grun LK, Teixeira NDR Jr, Mengden LV, et al. TRF1 as a major contributor for telomeres' shortening in the context of obesity. *Free Radic Biol Med*. 2018;129:286-295. <https://doi.org/10.1016/j.freeradbiomed.2018.09.039>
30. Peterson GL. Review of the Folin phenol protein quantitation method of Lowry, Rosebrough, Farr and Randall. *Anal Biochem*. 1979;100:201-220.
31. Heiss EH, Schilder YD, Dirsch VM. Chronic treatment with resveratrol induces redox stress- and ataxia telangiectasia-mutated (ATM)-dependent senescence in p53-positive cancer cells. *J Biol Chem*. 2007;282:26759-26766. <https://doi.org/10.1074/jbc.M703229200>
32. Lee J, Twomey M, Machado C, et al. Caveolae-mediated endocytosis of conjugated polymer nanoparticles. *Macromol Biosci*. 2013;13:913-920. <https://doi.org/10.1002/mabi.201300030>
33. Skehan P, Storeng R, Scudiero D, et al. New colorimetric cytotoxicity assay for anticancer-drug screening. *J Natl Cancer Inst*. 1990;82:1107-1112.
34. Andrade CM, Lopez PL, Noronha BT, et al. Ecto-5'-nucleotidase/CD73 knockdown increases cell migration and mRNA level of collagen I in a hepatic stellate cell line. *Cell Tissue Res*. 2011;344:279-286. <https://doi.org/10.1007/s00441-011-1140-7>
35. Justus CR, Leffler N, Ruiz-Echevarria M, Yang LV. In vitro cell migration and invasion assays. *J Vis Exp*. 2014;88:1-8. <https://doi.org/10.3791/51046>
36. Meira Martins L, Vieira M, Ilha M, et al. The interplay between apoptosis, mitophagy and mitochondrial biogenesis induced by resveratrol can determine activated hepatic stellate cells death or survival. *Cell Biochem Biophys*. 2014;71:1-16. <https://doi.org/10.1007/s12013-014-0245-5>
37. Urra H, Torres VA, Ortiz RJ, et al. Caveolin-1-enhanced motility and focal adhesion turnover require tyrosine-14 but not accumulation to the rear in metastatic cancer cells. *PLoS One*. 2012;7:1-14. <https://doi.org/10.1371/journal.pone.0033085>.
38. Grada A, Otero-Vinas M, Prieto-Castrillo F, Obagi Z, Falanga V. Research techniques made simple: analysis of collective cell migration using the wound healing assay. *J Invest Dermatol*. 2017;137:e11-e16. <https://doi.org/10.1016/j.jid.2016.11.020>
39. Maziveyi M, Alahari SK. Cell matrix adhesions in cancer: the proteins that form the glue. *Oncotarget*. 2017;8:48471-48487. <https://doi.org/10.18632/oncotarget.17265>
40. Yeh YC, Ling JY, Chen WC, Lin HH, Tang MJ. Mechanotransduction of matrix stiffness in regulation of focal adhesion size and number: reciprocal regulation of caveolin-1 and beta1 integrin. *Sci Rep*. 2017;7:1-14. <https://doi.org/10.1038/s41598-017-14932-6>.
41. Shi Y, Tan SH, Ng S, et al. Critical role of CAV1/caveolin-1 in cell stress responses in human breast cancer cells via modulation of lysosomal function and autophagy. *Autophagy*. 2015;11:769-784. <https://doi.org/10.1080/15548627.2015.1034411>
42. Shihata WA, Putra MRA, Chin-Dusting JPF. Is there a potential therapeutic role for caveolin-1 in fibrosis? *Front Pharmacol*. 2017;8:567-575. <https://doi.org/10.3389/fphar.2017.00567>.
43. DePascalis C, Etienne-Manneville S. Single and collective cell migration: the mechanics of adhesions. *Mol Biol Cell*. 2017;28:1833-1846. <https://doi.org/10.1091/mbc.E17-03-0134>
44. Luo X, Wang D, Zhu X, et al. Autophagic degradation of caveolin-1 promotes liver sinusoidal endothelial cells defenestration. *Cell Death Dis*. 2018;9:576-593. <https://doi.org/10.1038/s41419-018-0567-0>.
45. Nwosu ZC, Ebert MP, Dooley S, Meyer C. Caveolin-1 in the regulation of cell metabolism: a cancer perspective. *Mol Cancer*. 2016;15:71-83. <https://doi.org/10.1186/s12943-016-0558-7>.
46. Sinha B, Koster D, Ruez R, et al. Cells respond to mechanical stress by rapid disassembly of caveolae. *Cell*. 2011;144:402-413. <https://doi.org/10.1016/j.cell.2010.12.031>
47. Cheng JP, Nichols BJ. Caveolae: one function or many? *Trends Cell Biol*. 2016;26:177-189. <https://doi.org/10.1016/j.tcb.2015.10.010>
48. Martucci RB, Ziulkoski AL, Fortuna VA, et al. Beta-carotene storage, conversion to retinoic acid, and induction of the lipocyte phenotype in hepatic stellate cells. *J Cell Biochem*. 2004;92:414-423. <https://doi.org/10.1002/jcb.20073>
49. Bitencourt S, deMesquita FC, Caberlon E, et al. Capsaicin induces de-differentiation of activated hepatic stellate cell. *Biochem Cell Biol*. 2012;90:683-690. <https://doi.org/10.1139/o2012-026>

## SUPPORTING INFORMATION

Additional supporting information may be found online in the Supporting Information section.

**How to cite this article:** Ilha M, Moraes KdS, Rohden F, et al. Exogenous expression of caveolin-1 is sufficient for hepatic stellate cell activation. *J Cell Biochem*. 2019;120:19031-19043. <https://doi.org/10.1002/jcb.29226>